



Formulation and optimization of ivermectin nanocrystals for enhanced topical delivery

Hoda Awad^a, Mutasem Rawas-Qalaji^{a,b}, Rania El Hosary^c, Jayalakshmi Jagal^b, Iman Saad Ahmed^{a,b,*}

^a Department of Pharmaceutics & Pharmaceutical Technology, College of Pharmacy, University of Sharjah, Sharjah 27272, United Arab Emirates

^b Research Institute for Medical and Health Sciences, University of Sharjah, Sharjah 27272, United Arab Emirates

^c Department of Pharmaceutics, Egyptian Drug Authority, Cairo 12553, Egypt

ARTICLE INFO

Keywords:

Ivermectin
Nanocrystal
Antiparasitic
Dermal drug delivery
Quality by design (QBD)
Skin

ABSTRACT

The increasing resistance to antiparasitic drugs and limited availability of new agents highlight the need to improve the efficacy of existing treatments. Ivermectin (IVM) is commonly used for parasite treatment in humans and animals, however its efficacy is not optimal and the emergence of IVM-resistant parasites presents a challenge. In this context, the physico-chemical characteristics of IVM were modified by nanocrystallization to improve its equilibrium water-solubility and skin penetration, potentially improving its therapeutic effectiveness when applied topically. IVM-nanocrystals (IVM-NC) were prepared using microfluidization technique. The impact of several process/formulation variables on IVM-NC characteristics were studied using D-optimal statistical design. The optimized formulation was further lyophilized and evaluated using several in vitro and ex vivo tests. The optimal IVM-NC produced monodisperse particles with average diameter of 186 nm and polydispersity index of 0.4. In vitro results showed an impressive 730-fold increase in the equilibrium solubility and substantial 24-fold increase in dissolution rate. Ex vivo permeation study using pig's ear skin demonstrated 3-fold increase in dermal deposition of IVM-NC. Additionally, lyophilized IVM-NC was integrated into topical cream, and the resulting drug release profile was superior compared to that of the marketed product. Overall, IVM-NC presents a promising approach to improving the effectiveness of topically applied IVM in treating local parasitic infections.

1. Introduction

Dermatologic diseases rank as the fourth most prevalent cause of human illnesses (Tizek et al., 2019) and parasitic infections in particular are known to induce chronic diseases that can be more detrimental than bacterial infections (Sun et al., 2019). Specifically, parasitic skin infections are widespread and cause substantial disability, morbidity,

mortality, and healthcare expenses (Al Jalali and Zeitlinger, 2020; Heukelbach et al., 2005). Many parasitic diseases are listed by the World Health Organization (WHO) as Neglected Tropical Diseases (NTD), including Leishmaniasis, Lymphatic Filariasis, Schistosomiasis and others (CDC - Neglected Tropical Diseases, 2023). Topical treatment of skin diseases is generally preferred, as it enables higher localization of the drug at the site of infection compared to systemic administration,

Abbreviations: 2FI, 2-factor interaction; ANOVA, analysis of variance; BCS, biopharmaceutic classification system; CMA, critical material attributes; CMC, critical micelle concentration; CPP, critical process parameters; CQA, critical quality attributes; DLS, dynamic light scattering; FDA, food and drug administration; HPLC, high-performance liquid chromatography; IVM, Ivermectin; IVM-NC, Ivermectin-nanocrystals; IVM-NC-L, Ivermectin-nanocrystals lyophilized; IVM-NC-S, Ivermectin-nanocrystals suspension; IVM-PVA-PM, Ivermectin physical mixture with PVA; IVM-RM, Ivermectin raw material; IVM-SDS-PM, Ivermectin physical mixture with SDS; NC, nanocrystals; NTD, neglected tropical disease; PBS, phosphate buffered saline; PDA, photodiode-array; PDI, polydispersity index; PK, pharmacokinetics; PM, physical mixture; PS, particle size; PVA, poly(vinyl alcohol); QBD, quality by design; RH, relative humidity; SC, stratum corneum; SD, standard deviation; SDS, sodium dodecyl sulfate; SEM, scanning electron microscope; TEM, transmission electron microscopy; USP, United States pharmacopoeia; WHO, world health organization; XRD, X-ray diffraction; ZP, Zeta potential.

* Corresponding author at: Department of Pharmaceutics & Pharmaceutical Technology, College of Pharmacy, University of Sharjah, Sharjah 27272, United Arab Emirates.

E-mail addresses: U19104592@sharjah.ac.ae (H. Awad), mqalaji@sharjah.ac.ae (M. Rawas-Qalaji), jjagal@sharjah.ac.ae (J. Jagal), iahmed@sharjah.ac.ae (I.S. Ahmed).

<https://doi.org/10.1016/j.ijpx.2023.100210>

Received 27 May 2023; Received in revised form 3 September 2023; Accepted 5 September 2023

Available online 7 September 2023

2590-1567/© 2023 The Authors. Published by Elsevier B.V. This is an open access article under the CC BY-NC-ND license (<http://creativecommons.org/licenses/by-nc-nd/4.0/>).

which can result in higher toxicity and side effects. Additionally, topical administration is more patient-friendly and can result in better compliance. Therefore, topical antiparasitic agents are considered the most effective way to manage and control parasitic skin infections (Lipsky and Hoey, 2009; Das et al., 2020; Patel et al., 2018).

Ivermectin (IVM) is a mixture of avermectin A_{1a}, 5-O-demethyl-22,23-dihydro-(component H₂B_{1a}), and avermectin A_{1a}, 5-O-demethyl-25-de(1-methylpropyl)-22,23-dihydro-25-(1-methylethyl)-(component H₂B_{1b}) belonging to the macrocyclic lactone family (Sharun et al., 2019; USP, 2020). It is a broad-spectrum antiparasitic drug against a variety of parasites. It has been a popular drug of choice for the treatment of different types of parasite infestations, such as scabies, rosacea, head lice, trichuriasis, river blindness (onchocerciasis), lymphatic filariasis, and strongyloidiasis (Das et al., 2020; Atmakuri et al., 2023). It is available in several commercial forms including creams, lotions, and tablets, however, their effectiveness is limited due to IVM low water solubility and poor ability to penetrate the skin. IVM is classified as a Biopharmaceutics Classification System (BCS) Class II drug, and it is also a substrate for P-glycoprotein, which may assign it as BCS Class IV as well (Das et al., 2020; Starkloff et al., 2017). In treating parasitic infections such as scabies, where the parasites are located in the deeper layers of the skin, topical IVM has been found to be more effective compared to oral administration (Das et al., 2020). However, prolonged use of antiparasitic agents can lead to the emergence of resistant organisms (Bruschi, 2014). Therefore, it is crucial to develop new formulations that can improve IVM dermal delivery and enhance its antiparasitic efficacy.

Nano-formulations offer numerous advantages over conventional topical formulations, such as improved drug solubility, enhanced drug accumulation in the skin, and controlled drug release, leading to reduced frequency and dosage of topical application (Huh and Kwon, 2011; Kalhapure et al., 2015; Sharma et al., 2016). However, several challenges are associated with many nano-formulations, including low drug entrapment efficiency, poor permeability, stability issues related to degradation, and local irritation resulting from different excipients. Dendritic nanoparticles are one of the few nano-formulations that have been reported to effectively overcome the skin barrier while avoiding significant irritation (Agrawal et al., 2013; Kuchler et al., 2009). In contrast to nano-formulations, which require the nanoparticle to cross a biological membrane to deliver the loaded drug (Ahmed et al., 2018), the nanocrystal (NC) can simply form a supersaturated solution at the delivery site that aids its own direct diffusion through the skin, making them an appealing option for topical application. NC consist of 100% drug surrounded by a stabilizer layer and the simplicity of producing them for actives with poor water solubility is one of their major advantages (Rawas-Qalaji et al., 2015; Purohit et al., 2023). Additionally, NC facilitate deeper penetration into the skin layers, resulting in fewer side effects due to the limited inclusion of excipients. They are also highly reproducible and have lower manufacturing costs, making them an excellent choice for pharmaceutical companies (Junghanns and Müller, 2008; Mishra et al., 2009; Müller et al., 2011). NC <1 µm can penetrate the skin and accumulate in the hair follicles (Patzelt et al., 2011), with particles below 320 nm providing prolonged release and deeper penetration (Lademann et al., 2007). The significant surface area of NC that come in contact with the skin enables them to localize and achieve high concentration in the specific area of infection by forming a drug depot in the water phase of the skin environment (Junghanns and Müller, 2008; Mishra et al., 2009; Müller et al., 2011; Xing et al., 2010). This allows for enhanced drug delivery to deeper infection areas in the skin due to the creation of a higher concentration gradient, in accordance with Fick's law (Dragicevic and Maibach, 2016; Gigliobianco et al., 2018).

Previous studies have explored various dermal delivery routes for IVM, including solid lipid nanoparticles (Guo et al., 2018), lipid nanocapsules (Ullio-Gamboa et al., 2017), microemulsions (Das et al., 2020), and nanoemulsions (Da, 2015). However, to the best of our knowledge,

this research represents the first attempt to investigate the use of nanocrystals for reformulating IVM into a topical product to enhance its dermal delivery and antiparasitic efficacy. The objective of this work was to design, optimize, and characterize IVM-NC as a potential therapeutic alternative for the treatment of parasitic skin infections. The optimized formulation selected through statistical design was subjected to lyophilization to improve its physical stability and facilitate its incorporation into topical products, such as cream. This formulation was evaluated through a series of in vitro and ex vivo studies to determine its effectiveness compared to IVM raw material (IVM-RM) and physical mixtures (PM) of IVM with selected stabilizers. Furthermore, the optimized IVM-NC topical formulation was compared to the commercially available Soolantra Cream (10 mg/g, Galderma International), and its stability was assessed.

2. Materials and methods

2.1. Materials

IVM was received as a gift from Hovione PharmaScience Limited (Taipa, Macau). High Performance Liquid Chromatography (HPLC) grade Acetonitrile (Honeywell, Germany), Ethanol (Honeywell, Germany), Methanol (Sigma-Aldrich, France) and Orthophosphoric Acid 85% (VWR, France) were used. Also, the following chemicals were used: Acetic Acid (Sigma-Aldrich, Germany), Cetostearyl Alcohol (Spectrum Chemical MFG. CORP, USA), D-Mannitol (Sigma-Aldrich, China), Liquid Paraffin (Merck KGaA, Germany), Paraffin Wax (Sigma-Aldrich, Switzerland), Phosphate Buffered Saline (PBS) Tablet (Sigma-Aldrich, USA), Poly(vinyl alcohol) (PVA) with average molecular weight of 30,000–70,000 Da (Sigma-Aldrich, Netherlands), Propylene Glycol (Sigma-Aldrich, USA), Sodium Acetate Trihydrate (Sigma-Aldrich, Germany), Sodium Dodecyl Sulfate (SDS) (Sigma-Aldrich, Japan), Tween® 60 (Sigma Life Science, USA) and Tween® 80 (Sigma-Aldrich, Germany). Soolantra 1% w/w Cream (Lot No. 0414050, Expiry Date 09/2022, Galderma, France) was used in this study as a reference comparable product.

2.2. Quality by Design (QbD) for the optimization of IVM-NC

To create a novel formulation for a pre-existing drug, it is essential to recognize the potential Critical Material Attributes (CMAs) and Critical Process Parameters (CPPs) and have a clear understanding of how they influence the desired Critical Quality Attributes (CQAs) of the final product. In this study, D-optimal response surface design was utilized to optimize IVM-NC using Design-Expert® software (Version 13.0, Stat-Ease Inc., Minneapolis, MN, USA). Three numerical discrete factors and two categorical factors were chosen as CMAs/CPPs to investigate their impact on the selected CQAs. These factors were: (1) number of microfluidization cycles (X₁), (2) drug concentration (X₂), (3) stabilizer to drug ratio (X₃), (4) type of stabilizer (X₄) and (5) homogenization prior to microfluidization (X₅). The levels of independent variables were

Table 1

The independent variables (factors) and dependent variables (responses) for the optimization of Ivermectin nanocrystals (IVM-NC).

Numerical Factors (discrete)		Applied Levels		
X ₁	Number of microfluidization cycles	1	3	5
X ₂	Drug concentration (% w/v)	0.025	0.05	0.1
X ₃	Stabilizer to drug ratio (w/w)	1:1	2:1	4:1
Categorical Factors		Applied Levels		
X ₄	Type of stabilizer	PVA	SDS	Tween® 80
X ₅	Homogenization prior to microfluidization	Yes	No	
Responses		Optimization Goal		
Y ₁	PS	Minimize		
Y ₂	PDI	Minimize		
Y ₃	Absolute ZP	Maximize		

chosen in a way that ensures an appropriate design space while also allowing for feasible processing of the NC. (Table 1). Three responses were selected to monitor closely for the optimization of the studied factors: (1) particle size (PS, Y_1), (2) polydispersity index (PDI, Y_2) and (3) Zeta Potential (ZP, Y_3). IVM-NC formulations were optimized for the three responses with a target of achieving the smallest PS, lowest PDI and highest ZP to obtain the highest overall desirability value. The optimal independent variables were then used to prepare the optimal IVM-NC for further testing and incorporation into the topical cream.

Table 2 presents 34 experimental runs (formulations) generated by the Design-Expert® software, which includes five replications. All responses were fitted concurrently to linear, two-factor interaction (2FI) and quadratic response surface models. The resulting polynomial equations were subjected to automatic statistical validation using analysis of variance (ANOVA), and interactions of three or higher order were disregarded for simplicity. Statistical parameters such as p-value, lack-of-fit p-value, adjusted multiple correlation coefficient (Adjusted- R^2), predicted multiple correlation coefficient (Predicted- R^2), and multiple correlation coefficient (R^2) were assessed to ensure the significance of the selected model. The model with the maximum Adjusted- R^2 and Predicted- R^2 with a minimal difference between the two parameters and an insignificant lack of fit, was selected. To enhance the model's predictability and eliminate any potential bias, the experimental runs were conducted in random order.

2.3. Selection of the optimal formulation

The chosen model for response prediction was assessed for its significance, and 3D-response surface plots were generated for each response to assess the degree of factor interaction. The outcomes were

Table 2

The experimental design and measured responses for the optimization of IVM-NC.

Formulation	X_1 (cycles)	X_2 (%)	X_3 (ratio)	X_4 (type)	X_5 (homogenization)	Y_1 : PS (nm)	Y_2 : PDI	Y_3 : ZP (mV)
F1	1	0.025	4:1	SDS	Yes	131.9 ± 93.2	0.74 ± 0.25	-18.5 ± 0.8
F2	5	0.025	1:1	SDS	Yes	278.2 ± 16.9	0.93 ± 0.06	-30.2 ± 1.1
F3	1	0.1	4:1	SDS	No	11.5 ± 0.9	0.73 ± 0.29	-34.2 ± 12.2
F4	3	0.1	2:1	Tween® 80	No	301.3 ± 50.0	0.88 ± 0.12	-13.0 ± 1.3
F5	5	0.025	4:1	SDS	No	242.6 ± 59.5	0.74 ± 0.25	-10.3 ± 5.4
F6	1	0.1	4:1	PVA	Yes	338.5 ± 81.9	0.84 ± 0.18	-9.4 ± 1.3
F7	5	0.025	4:1	PVA	Yes	437.0 ± 186.9	0.97 ± 0.05	-18.2 ± 2.3
F8	1	0.025	4:1	Tween® 80	No	9.1 ± 0.5	0.97 ± 0.04	-6.0 ± 1.0
F9	3	0.05	1:1	Tween® 80	No	198.4 ± 33.9	0.95 ± 0.09	-13.6 ± 0.5
F10	1	0.1	2:1	Tween® 80	Yes	213.2 ± 153.8	0.97 ± 0.04	-18.9 ± 0.8
F11	5	0.05	1:1	SDS	No	325.4 ± 28.3	0.72 ± 0.04	-33.9 ± 0.6
F12	5	0.025	1:1	PVA	No	416.8 ± 140.5	0.95 ± 0.08	-16.5 ± 0.4
F13	1	0.025	1:1	Tween® 80	Yes	246.1 ± 24.9	0.97 ± 0.04	-18.4 ± 1.5
F14	5	0.025	2:1	Tween® 80	No	301.1 ± 72.9	0.97 ± 0.04	-17.5 ± 3.9
F15	3	0.025	2:1	PVA	Yes	446.1 ± 68.2	0.99 ± 0.03	-13.1 ± 0.7
F16	1	0.025	1:1	SDS	No	168.1 ± 143.7	0.74 ± 0.25	-2.8 ± 1.8
F17	1	0.05	2:1	SDS	Yes	215.8 ± 54.2	0.74 ± 0.25	-40.6 ± 0.3
F18	1	0.025	2:1	Tween® 80	No	230.0 ± 73.9	0.97 ± 0.04	-9.7 ± 1.5
F19	5	0.05	4:1	Tween® 80	Yes	517.5 ± 487.9	0.91 ± 0.15	-3.1 ± 1.1
F20	1	0.1	4:1	SDS	No	13.5 ± 1.2	0.60 ± 0.19	-47.5 ± 1.9
F21	1	0.05	4:1	PVA	No	393.4 ± 153.4	0.91 ± 0.17	-22.9 ± 0.4
F22	5	0.025	1:1	SDS	Yes	228.4 ± 14.3	0.94 ± 0.07	-37.8 ± 3.9
F23	5	0.1	1:1	SDS	No	351.8 ± 5.6	0.49 ± 0.05	-36.6 ± 3.0
F24	5	0.1	4:1	SDS	Yes	292.2 ± 173.7	0.40 ± 0.10	-38.9 ± 2.3
F25	5	0.1	2:1	PVA	Yes	672.7 ± 85.8	0.56 ± 0.11	-19.7 ± 1.1
F26	1	0.1	1:1	PVA	No	457.1 ± 154.6	0.62 ± 0.54	-9.4 ± 1.4
F27	5	0.1	1:1	Tween® 80	Yes	139.7 ± 53.1	0.97 ± 0.04	-8.7 ± 0.7
F28	5	0.1	4:1	SDS	Yes	81.2 ± 2.5	0.22 ± 0.01	-38.0 ± 1.0
F29	1	0.1	1:1	SDS	Yes	347.5 ± 27.9	0.78 ± 0.07	-47.4 ± 3.3
F30	5	0.1	4:1	Tween® 80	No	177.4 ± 35.4	0.97 ± 0.04	-16.4 ± 2.4
F31	3	0.05	2:1	SDS	No	239.0 ± 26.6	0.60 ± 0.05	-52.3 ± 3.8
F32	1	0.1	1:1	PVA	No	390.9 ± 55.6	0.89 ± 0.18	-14.9 ± 0.6
F33	5	0.025	1:1	PVA	No	438.8 ± 45.3	0.94 ± 0.06	-21.6 ± 0.4
F34	3	0.1	4:1	PVA	No	677.2 ± 73.7	0.56 ± 0.09	-19.6 ± 0.9

X_1 : Number of microfluidization cycles, X_2 : Drug concentration (% w/v), X_3 : Stabilizer to drug ratio (w/w), X_4 : Stabilizer type, X_5 : Homogenization prior to microfluidization.

visually examined. The optimal values for the dependent variables were determined based on the criteria of the smallest PS, lowest PDI, and highest absolute ZP. For optimization, both numerical and graphical analyses were carried out utilizing the desirability function. Desirability values range from 0 to 1, and values closer to 1 were reported to indicate the most desired response (Oscar et al., 2019). After selecting the optimal IVM-NC preparation, further investigations were conducted.

2.4. Preparation of IVM-NC

2.4.1. Preparation of IVM-NC suspensions

In accordance with the experimental design, IVM-NC were prepared using a top-down approach via the microfluidization technique (Rawas-Qalaji et al., 2015; Verma et al., 2009). Increasing amounts of IVM (ranging from 0.0125 mg to 0.05 mg) and Food and Drug Administration (FDA) approved, biocompatible stabilizers such as Tween® 80, PVA, and SDS were added to 50 mL of purified water, to result in a drug concentration range of 0.025% to 0.1% (w/v) and a stabilizer-to-drug ratio of 1 to 4. The resulting mixture was then processed in a microfluidizer (M-110P V3, Microfluidics Corporation, USA) under a pressure of 30,000 psi for 1 to 5 cycles. In instances where homogenization was necessary as per the experimental design, the mixture was homogenized prior to microfluidization at 10,000 rpm for 10 min using a high-speed homogenizer (T-25 digital Ultra Turrax, IKA-Werke GmbH & Co., Germany).

2.4.2. Preparation of freeze-dried IVM-NC

After selecting the optimal IVM-NC suspension (IVM-NC-S) using the experimental design, it was combined with 1% mannitol as a cryoprotectant and frozen at -80 °C using the Innova U725-G freezer (New

Brunswick Scientific, Canada). The frozen nanosuspension was then subjected to lyophilization using a freeze drier (VirTis BenchTop Pro with Omnitronics™, USA) at $-102\text{ }^{\circ}\text{C}$ and 200 mT for 36 h to obtain dry powder lyophilizate (IVM-NC-L).

2.4.3. Preparation of IVM-NC topical cream

To compare the drug release of the lyophilized IVM-NC (IVM-NC-L) with the commercial product Soolantra Cream (1% w/w IVM, Galderma, France), the IVM-NC-L was incorporated into a cream formulation. The IVM-NC cream was composed of 1% IVM (w/w), 4.1% (w/w) liquid paraffin, 48% (w/w) white soft paraffin ointment, 10% (w/w) propylene glycol, and 36.9% (w/w) water containing 0.21% citric acid (Ahmed et al., 2020).

2.5. Micromeritics of IVM-NC

2.5.1. Particle size, polydispersity index and zeta potential

The Malvern Instruments' Zetasizer Nano ZS-90 utilizing photon correlation spectroscopy dynamic light scattering (DLS) was used to determine the average PS, PDI, and ZP. Prior to analysis, the IVM-NC-S samples were suitably diluted with purified water, while IVM-NC-L samples were redispersed then diluted in purified water. Additionally, the surface charge of the optimal IVM-NC was quantified by measuring the ZP at a scattering angle of 173° and a temperature of $25\text{ }^{\circ}\text{C}$. The mean value \pm standard deviation (SD) of three replicates was calculated ($n = 3$).

2.6. Physico-chemical characterization of optimal IVM-NC

2.6.1. Determination of equilibrium solubility

To determine the equilibrium solubility of IVM raw material (IVM-RM), IVM physical mixture with SDS (IVM-SDS-PM), and the optimal IVM-NC-L formulation, the shaking flask method was employed (USP 1236 general chapter). In this method, an excess amount of powders equivalent to 10 mg IVM was taken from each sample and added to conical flasks containing 10 mL of acetate buffer ($\text{pH} = 5.5$) to ensure supersaturation conditions. The flasks were placed in a benchtop shaking incubator (Labnet International Inc., USA) and shaken at 50 rpm at room temperature for 24 h to reach equilibrium. The resulting samples were filtered through a $0.2\text{ }\mu\text{m}$ filter, diluted with acetate buffer ($\text{pH} = 5.5$) as required, and analyzed for IVM concentration at 240 nm using a microplate reader (Synergy H1, BioTek, USA). The concentration of the dissolved IVM was calculated using the calibration curve equation and then plotted against time. The regression equation for the calibration curve was as shown in eq. (1) with a regression coefficient of $R^2 = 0.9901$ and the assay was linear in the concentration range of 2–20 $\mu\text{g}/\text{mL}$. All tests were conducted in triplicates ($n = 3$).

$$y = 27301x - 0.0022 \quad (1)$$

2.6.2. In vitro dissolution studies

The United States Pharmacopoeia (USP) monograph method was employed to establish the dissolution profiles of the previously prepared samples outlined in section 2.6.1 (IVM-RM, IVM-SDS-PM, IVM-NC-L), which were equivalent to 20 mg of IVM. A USP paddle apparatus (ERWEKA DT820 Dissolution Apparatus, ERWEKA GmbH, Germany) was used for the dissolution tests, which were conducted at $32\text{ }^{\circ}\text{C}$ in 900 mL of acetate buffer solution with a pH of 5.5, which is the pH of normal skin (Sheshala et al., 2019). Samples of 3 mL were taken at different time intervals (5, 10, 15, 20, 25, 30, 35, 40, 45, and 60 min) and replaced with an equal volume of acetate buffer ($\text{pH} = 5.5$). The samples were then filtered through a $0.2\text{ }\mu\text{m}$ syringe filter and analyzed for drug content at 240 nm using a microplate reader (Synergy H1, BioTek, USA). The dissolved drug percentage was determined using the calibration curve equation as before and then plotted against time. All tests were conducted in triplicates ($n = 3$).

2.6.3. X-ray diffraction (XRD)

Powder XRD patterns of IVM-RM, SDS, IVM-SDS-PM in 1:4 ratio, and the optimal IVM-NC-L were determined using an X-ray diffractometer (D8 Advance, Bruker, Germany). Diffractograms were created using a Cu radiation source ($\lambda = 1.5418\text{ \AA}$) with a maximum voltage of 40 kV and a maximum current of 40 mA over the 2θ range of 5° to 60° .

2.7. Morphological characterization

The morphology of the optimal IVM-NC-S as well as IVM-NC-L were determined by transmission electron microscopy (TEM) operated at a voltage of 200 kV. The sample was loaded on a copper-gold carbon grid and left to be air-dried at room temperature. Then, the grid was placed in the vacuum chamber of the electron microscope (JEOL-2100, Jeol Ltd., Tokyo, Japan) and images were captured using different magnification powers (Shen et al., 2018). The IVM-RM was captured through scanning electron microscope (SEM). To prepare the SEM sample, a small amount of dispersed IVM-RM was placed on a clean slide cover and allowed to dry in a vacuum. Afterwards, the sample was attached to carbon tape and coated with gold using a high vacuum sputter module. The coated sample was then scanned, and images were captured using a 3 kV acceleration voltage (Thermo Scientific Apreo SEM, FEI Company, Hillsboro, OR, USA).

2.8. Short-term physical stability study

The physical stability of the optimal IVM-NC-S and IVM-NC-L was evaluated for a period of three months at two different storage conditions: $25\text{ }^{\circ}\text{C}/60\%$ relative humidity (RH) using a Climacell stability chamber (MMM Group, Germany) and $5 \pm 3\text{ }^{\circ}\text{C}$ using a refrigerator. Prior to storage and after 1, 2 and 3 months, the PS, PDI and ZP of the samples were analyzed. The stability samples were freshly prepared and stored in glass vials wrapped in aluminum foil. All measurements were conducted in triplicates ($n = 3$) (Starkloff et al., 2017; Verma et al., 2009).

2.9. Ex vivo studies: skin permeation of IVM-NC

The ex vivo permeation studies were carried out using six Franz cells and a V-series stirrer (V6-CB, PermeGear, USA), as previously reported (Rawas-Qalaji et al., 2015; Aodah et al., 2017; Bafail et al., 2019; Najm et al., 2022). To maintain the integrity of the stratum corneum (SC) lipids, temperature control at $32 \pm 0.5\text{ }^{\circ}\text{C}$ was crucial and achieved using a water bath (JULABO GmbH, BC4, Germany). Adult pig ear skin was obtained from a local butcher (Ajman, UAE) and used for the study due to its comparable structural and permeation kinetics with human skin. The dorsal skin was separated from the underlying cartilage with forceps and scalpel (blades No. 20 and 11), and cleaned to remove the subcutaneous fat, hair, and blood vessels. The selected intact skin patches were washed with PBS ($\text{pH} = 7.4$), wrapped in aluminum foil, and stored at $-20\text{ }^{\circ}\text{C}$. Prior to the study, the frozen skin was moistened with PBS ($\text{pH} = 7.4$) until completely defrosted at ambient temperature and placed on Franz cells with a diffusional area of 3.14 cm^2 . The skin patches were divided into two sets, where only one of them was soaked in a solution of acetonitrile and water in the ratio of 3.5:6.5 for 24 h before the experiment (treated skin), while the other set was not exposed to the organic solvent (untreated skin). In order to assess the impact of the organic solvent utilized in IVM solution preparation on the skin integrity, the experiment was conducted on IVM-NC-S using both treated and untreated skin simultaneously. The SC faced the donor compartments, which were filled with 3 mL of IVM-NC-S or IVM solution (prepared in acetonitrile and water in the ratio of 3.5:6.5), while the receptor compartments were filled with 15 mL of PBS ($\text{pH} = 7.4$). Samples of 100 μL were taken from the receptor medium and replaced with fresh medium at specific intervals (1, 2, 4, 8, 12, and 24 h), followed by HPLC analysis. The cumulative drug concentration that

permeated into the receptor medium was plotted against time. All experiments were done in triplicates ($n = 3$), and the mean values (\pm SD) were recorded.

2.10. In vitro release studies

To compare the release of IVM from the compounded IVM-NC cream (1% w/w IVM) to marketed Soolantra Cream (1% w/w IVM), in vitro release experiments were conducted. The study utilized a water bath shaker (Grant OL5 Aqua Pro, UK) and involved placing equal amounts of both creams (0.5 g) in dialysis bags (cellulose membrane, Mw cut off 14,000 Da, Sigma-Aldrich, USA) that were properly tightened. The bags were then placed in 250 mL conical flasks filled with 250 mL PBS (pH = 7.4) (Ahmed et al., 2020; Najm et al., 2022) to mimic the conditions of infected skin, at a temperature of 32 °C. The samples were shaken at 100 rpm to minimize the unstirred water layer effect. At 10-, 30-, 60- and 120-min intervals, samples of 3 mL were withdrawn from each flask and replaced with equal volumes of PBS (pH = 7.4). The samples were then filtered through 0.2 μ m filter and analyzed for IVM content by a microplate reader (Synergy H1, BioTek, Germany) at 240 nm (D'Souza, 2014). The concentration of the released drug was determined and plotted against time. The measurements were conducted in triplicates ($n = 3$).

2.11. HPLC analysis

An isocratic reversed-phase validated HPLC method (USP, 2020) was used for the detection and quantification of IVM using photodiode-array (PDA) detector (Waters Nova Framingham, MA, USA) equipped with a quaternary pump, auto-sampler unit, and UV detector set at 254 nm. The stationary phase was a reversed-phase C18 column (4 μ m particles size) (Waters Nova-Pak C18, Framingham, MA, USA). The mobile phase was a mixture of acetonitrile, methanol and water (53:27.5:19.5) and the flow rate was 1 mL/min. The mobile phase was filtered through a 0.45 μ m pore-size membrane filter. The run time was 5 min, and the injection volume was 10 μ L. The regression equation for the calibration curve was as shown in eq. (2) with a regression coefficient of $R^2 = 0.9997$. The assay was linear in the concentration range of 0.0625–1.0 mg/mL.

$$y = 3E + 06 x - 61090 \quad (2)$$

2.12. Statistical analysis

All measurements were carried out in triplicates and values were presented as mean \pm SD. Statistical analysis was conducted using Prism 9 (Version 9.5.1, GraphPad Software, San Diego, CA, USA). A two-tailed unpaired Student's *t*-test was used to compare two groups, while one-way ANOVA followed by Tukey post hoc test was employed for multiple comparisons. A *p*-value <0.05 was considered statistically significant.

3. Results and discussion

3.1. Preparation and optimization of IVM-NC

Nanocrystals are small particles that typically fall within the nanometer size range. They are comprised entirely of active material and are enveloped by a stabilizer layer, which serves to prevent their aggregation. NC provide a substantial advantage over other drug delivery systems, particularly when high therapeutic concentrations are necessary in targeted areas of the body. In topical formulations, reducing the particle size of NC can substantially increase their surface area of contact with the skin, improve drug supersaturation solubility, enhance drug release rate, improve skin surface adhesion, and boost dermal drug delivery through the skin barrier (Ghasemiyeh and Mohammadi-Samani, 2020; Liu et al., 2023).

In this study, IVM-NC were optimized by applying the experimental QbD approach. The CPPs and CMAs, and their potential impact on the desired CQAs were determined based on our knowledge of the NC formulation and the important variables as reported in literature (Starkloff et al., 2017; Verma et al., 2009; Najm et al., 2022; Li et al., 2018; Parmar and Bansal, 2021). IVM-NC were produced using a top-down micronization approach through microfluidization technique which is capable of forming very fine crystals (Patel et al., 2018). The configuration of the prepared 34 IVM-NC formulations which were generated using the D-optimal response surface design are summarized in Table 2. The assessment of the impact of number of microfluidization cycles (X_1), concentration of the drug (X_2), stabilizer to drug ratio (X_3), stabilizer type (X_4), homogenization prior to microfluidization (X_5) and their interactions on the produced IVM-NC resulted in PS ranging from 9 to 677 nm with PDI ranging from 0.216 to 0.985 and ZP in the range of -2.8 to -52.3 mV. These broad ranges indicate that the factors selected for the optimization process had a significant impact on the response variables.

Statistical analysis of the experimental design resulted in a mathematical expression in the form of a second order polynomial equation for each of the three responses PS, PDI and ZP. The equations report the values of the intercept coefficient and the regression coefficients of the studied factors (X_1 - X_5) as described below:

$$\begin{aligned} \text{PS} = & 302.71 + 52.2 \times X_1 - 19.54 \times X_3 + 171.75 \times X_4 - 95.65 \times X_5^2 + 45.18 X_1 X_3 \\ & + 43.35 X_3 X_4 - 57.24 (X_3 X_4)^2 \end{aligned} \quad (3)$$

$$\begin{aligned} \text{PDI} = & 0.8157 - 0.0409 \times X_1 - 0.0948 \times X_2 - 0.0284 \times X_3 - 0.0017 \times X_4 - 0.1492 (X_4)^2 \\ & - 0.0121 \times X_5 - 0.0662 X_1 X_2 - 0.0538 X_2 X_4 - 0.0299 (X_2 X_4)^2 + 0.0381 X_3 X_5 \end{aligned} \quad (4)$$

$$\begin{aligned} \text{ZP} = & -20.8 - 0.6945 \times X_1 - 3.53 \times X_2 + 1.31 \times X_3 + 4.49 \times X_4 - 12.58 (X_4)^2 \\ & + 0.5435 \times X_5 \end{aligned} \quad (5)$$

The models selected for further analysis were based on the outcome of the experimental design as summarized in Table 3. These models were significant ($p < 0.05$) and exhibited maximum adjusted R^2 that was within a reasonable agreement with the predicted R^2 and had insignificant lack of fit. The statistical analysis of the measured responses from the 34 experimental runs suggests reduced 2FI model to be the most suitable to describe the effect of the studied factors on PS and PDI, while the linear model best fits the effect on ZP with high efficiency. The graphical representation of the relationship between the studied factors and the responses are presented in Figs. 1-3.

3.1.1. Effect of studied factors on the responses

To achieve a successful and efficient topical formulation containing IVM-NC, it is crucial to produce monodisperse populations of IVM-NC with a specific size. The PS and PDI of IVM-NC are crucial when applying them topically on the skin. These factors can impact the supersaturation solubility of the active in the aqueous phase of the skin, the biodistribution and retention of the NC in the skin layers, as well as the diffusion and permeation of the active through the skin layers. Ultimately, this can impact the local bioavailability of IVM at the infection site and the potential uptake by parasitic cells. Additionally, the zeta potential (ZP) of the NC plays a vital role in stabilizing the nano-suspension upon storage and facilitating the redispersion of the dried NC.

3.1.1.1. Number of microfluidization cycles (X_1). The impact of the number of microfluidization cycles on the production of NC has been extensively studied, with higher numbers of cycles resulting in longer

Table 3

The outcome of the experimental design.

Response	Model	R ²	Adjusted R ²	Predicted R ²	Lack of fit p-value	Model p-value	Most significant terms
PS (nm)	Reduced 2FI	0.7146	0.6378	0.4298	0.2165	<0.0001	X ₁ (<i>p</i> = 0.0127) X ₄ (<i>p</i> < 0.0001) X ₁ X ₃ (<i>p</i> = 0.0351)
PDI	Reduced 2FI	0.864	0.8048	0.6884	0.8608	<0.0001	X ₁ (<i>p</i> = 0.0261) X ₂ (<i>p</i> < 0.0001) X ₄ (<i>p</i> < 0.0001) X ₁ X ₂ (<i>p</i> = 0.0017) X ₂ X ₄ (<i>p</i> = 0.0117) X ₃ X ₅ (<i>p</i> = 0.0436) X ₄ (<i>p</i> < 0.0001)
ZP (mV)	Linear	0.5601	0.4624	0.3108	0.066	0.0006	

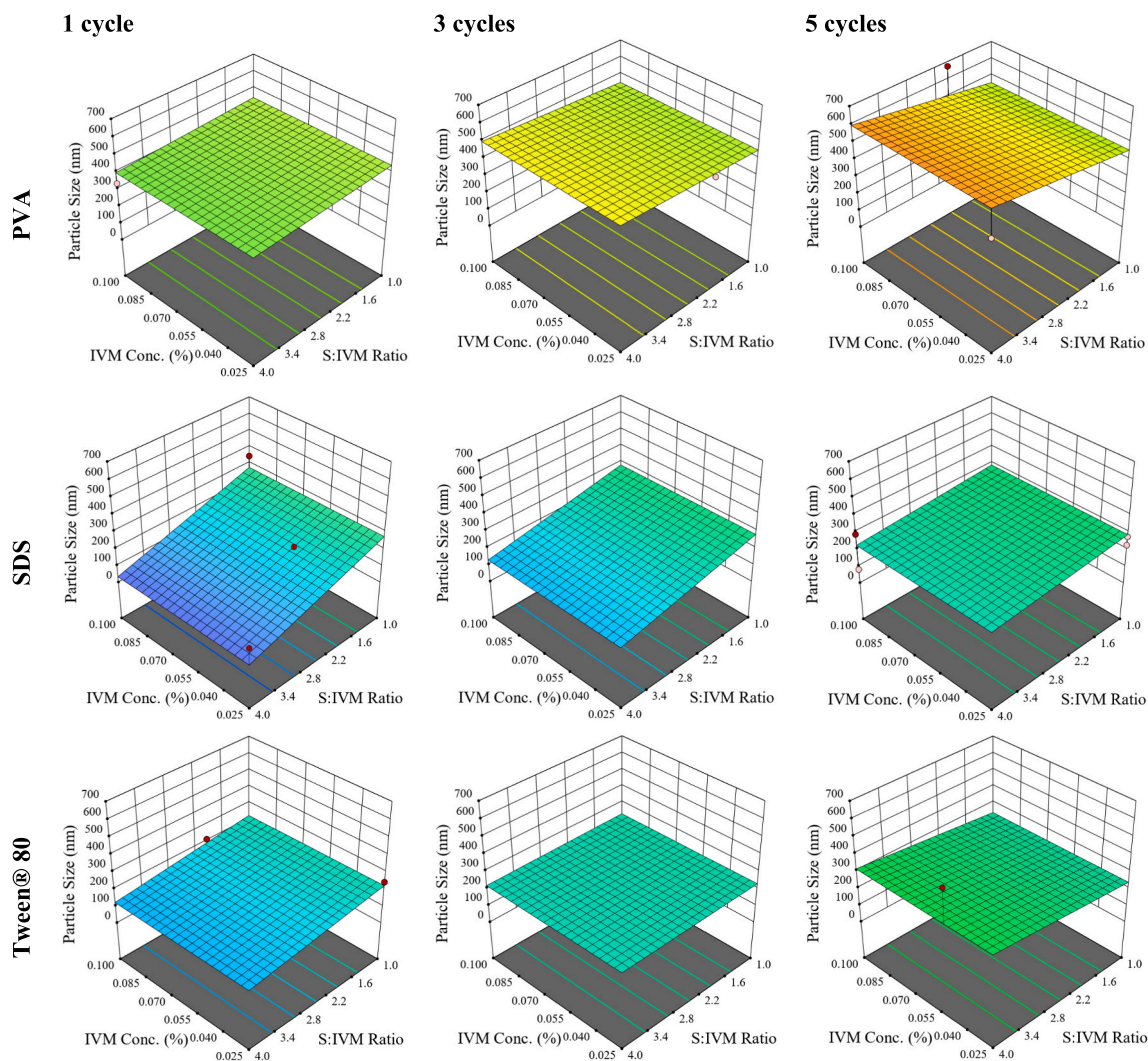


Fig. 1. Response surface plots for the effects of IVM concentration (IVM Conc.) and stabilizer to drug ratio (S:IVM Ratio) on PS with processing for different number of microfluidization cycles using PVA, SDS and Tween® 80 as stabilizers.

drug shearing time. This factor has been found to have a significant impact on the PS, as evidenced by a *p*-value of 0.0127, and a lesser impact on the PDI, with a *p*-value of 0.0261. In microfluidization, the main parameter affecting PS is shearing time, provided that pressure is held constant. Therefore, it is expected that increasing the number of microfluidization cycles will result in smaller PS. However, it has been reported that at high pressure, the extent of PS reduction is significant at the beginning of the shearing process and plateaus with prolonged shearing time. If the drug is exposed to excessive shearing for prolonged time, the PS will start to increase as the crystals become depleted of the

stabilizer, leading to aggregation due to high surface free energy (Verma et al., 2009).

There was moderate evidence of a 2-FI effect between the number of microfluidization cycles and the stabilizer to drug ratio (X₁X₃) on PS, with a *p*-value of 0.0351. When the stabilizer ratio is increased while decreasing the number of cycles, lower PS are observed for all stabilizers.

Another significant 2-FI effect was found between the number of microfluidization cycles and the drug concentration (X₁X₂, *p* = 0.0017) on PDI. Increasing both factors lead to smaller PDI values. Overall, the

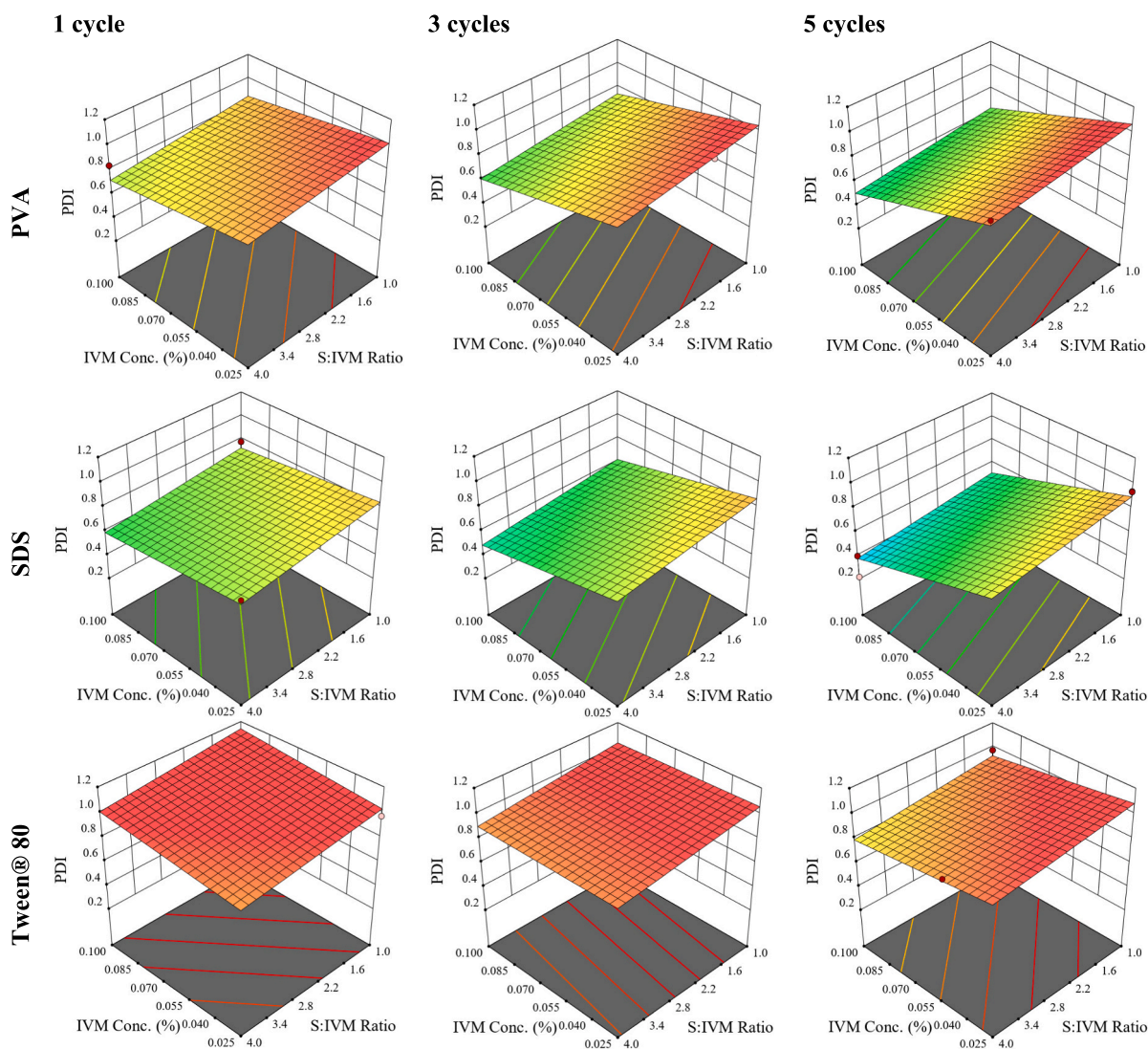


Fig. 2. Response surface plots for the effects of IVM concentration (IVM Conc.) and stabilizer to drug ratio (S:IVM Ratio) on PDI with processing for different number of microfluidization cycles using PVA, SDS and Tween® 80 as stabilizers.

number of microfluidization cycles is an essential factor to consider when producing NC, as it has a significant impact on PS and can interact with other factors, such as stabilizer ratio and drug concentration.

3.1.1.2. Drug concentration (X_2). The concentration of IVM in the liquid dispersion had a highly significant main effect ($p < 0.0001$) on the PDI values. This can be explained by the fact that higher drug concentrations lead to increased shear forces in the microfluidizer, maximizing particle collision and resulting in better size distribution of the final product. Additionally, increasing the drug concentration results in a larger population of particles which might reduce the variability and improve the PDI result. Furthermore, drug concentration had a significant 2-FI effect with the number of microfluidization cycles on PDI (X_1X_2 , $p = 0.0017$), as discussed in section 3.1.1.1. There was also a significant 2-FI effect with stabilizer type (X_2X_4 , $p = 0.0117$), where increasing drug concentration resulted in lower PDI values when PVA or SDS were used. In contrast, increasing drug concentration with Tween® 80 led to higher PDI values.

3.1.1.3. Stabilizer to drug ratio (X_3). The stabilizer to drug ratio in the formulation plays a crucial role in the formation of a stable nanosuspension. If the stabilizer concentration is lower than required, the formed NC might not be adequately covered leading to aggregation

(Verma et al., 2009). The stabilizer to drug ratio showed no significant main effects on the three responses indicating that the range of ratios used were all appropriate and that the type rather than the ratio might play a more important role. Similar results were previously reported for mupirocin nanocrystals (Najm et al., 2022). In terms of interactions, only a 2-FI effect with the number of microfluidization cycles (X_1X_3) had a minimal impact on PS ($p = 0.0351$) as discussed in section 3.1.1.1. No other significant interactions were observed with the studied factors.

3.1.1.4. Stabilizer type (X_4). The selection of stabilizers for the formation of the NC was done with the aim of choosing stabilizers from different classes with varying chemical and physicochemical properties to better understand their impact on the formulation (Verma et al., 2009). Therefore, the anionic surfactant SDS, the nonionic surfactant Tween® 80 and the polymeric PVA were selected.

The type of stabilizer used in the fabrication of the NC had the most significant impact on all three responses ($p < 0.0001$ for all responses). Experimental runs prepared with SDS as the stabilizer showed an overall larger ZP values compared to PVA and Tween® 80. This is due to the anionic nature of SDS, which imparts a negative charge to the IVM crystals when adsorbed on the surface (Verma et al., 2009), resulting in a stable nanosuspension with minimized PS and PDI. On the other hand, PVA resulted in an overall larger PS with high PDI, while Tween® 80

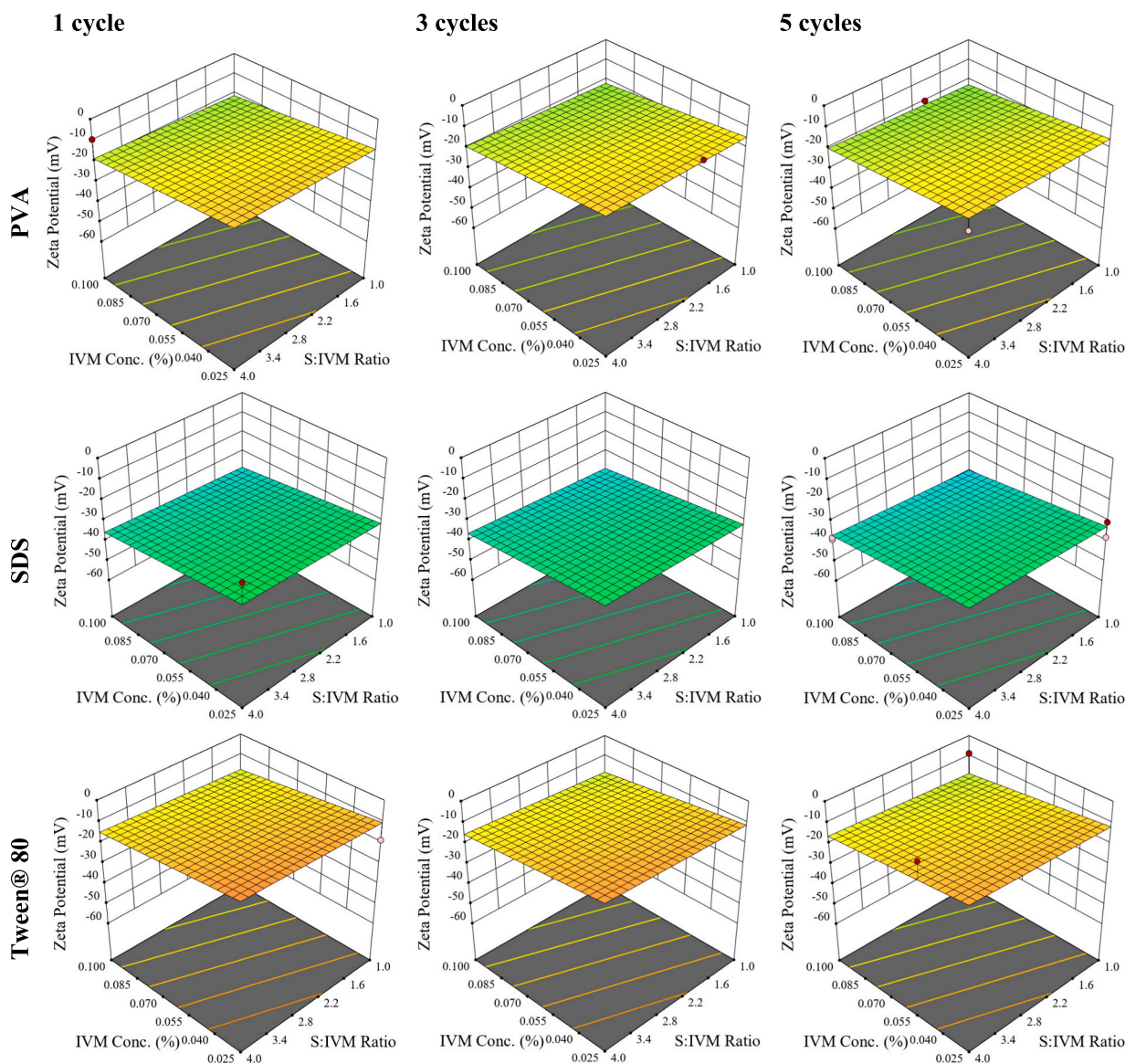


Fig. 3. Response surface plots for the effects of IVM concentration (IVM Conc.) and stabilizer to drug ratio (S:IVM Ratio) on ZP with processing for different number of microfluidization cycles using PVA, SDS and Tween® 80 as stabilizers.

yielded PS comparable to SDS but with higher PDI values. This factor also had a 2-FI effect with drug concentration, with a moderate impact on PDI (X_2X_4 , $p = 0.0117$) as discussed in [section 3.1.1.2](#).

3.1.1.5. Homogenization prior to microfluidization (X_5). The results indicate that homogenizing the liquid dispersion of IVM before introducing it into the microfluidizer had minimal impact on the three responses. The only significant effect observed was a 2-FI between stabilizer to drug ratio and homogenization prior to microfluidization (X_3X_5) on the PDI with a p -value of 0.0436. The data suggests that applying homogenization while increasing the stabilizer to drug ratio led to lower PDI. It is possible that the speed (10,000 rpm) used in the homogenization process contributed to this result. Nonetheless, homogenization was found to be useful in achieving proper dispersion of the samples prior to their introduction into the microfluidizer. This is especially advantageous to ensure more uniform flow and collision in the reaction chamber and to avoid clogging the microfluidic channels at higher drug concentrations.

3.2. Selection of the optimal IVM-NC formulation

The response surface analysis of the D-optimal design was utilized to optimize the preparation of IVM-NC formulation with desired CQAs. The goal was to minimize the PS and PDI while maximizing the absolute ZP of IVM-NC. The PDI represents the width of particle size distribution of IVM-NC, where values closer to 0 indicate monodisperse NC distributions (Nidhi et al., 2019). A narrow PDI minimizes the variability in equilibrium solubility between particles of different sizes, and consequently minimizes Ostwald ripening (Starkloff et al., 2017). Also, particles with ZP values in the range of -10 to $+10$ mV are considered neutral while particles with ZP of more than $+30$ or less than -30 are preferred to ensure particles repulsion, thus preventing their aggregation (Clogston and Patri, 2011). To achieve this, a simultaneous optimization approach was employed, where the highest priority value was assigned for PS, followed by PDI then ZP.

Based on the optimization results, the IVM-NC formulation prepared with SDS as a stabilizer in a 4:1 SDS to IVM ratio and a concentration of 0.1% (w/v) IVM was found to be the most desirable. The formulation was homogenized and microfluidized for three cycles. The optimized

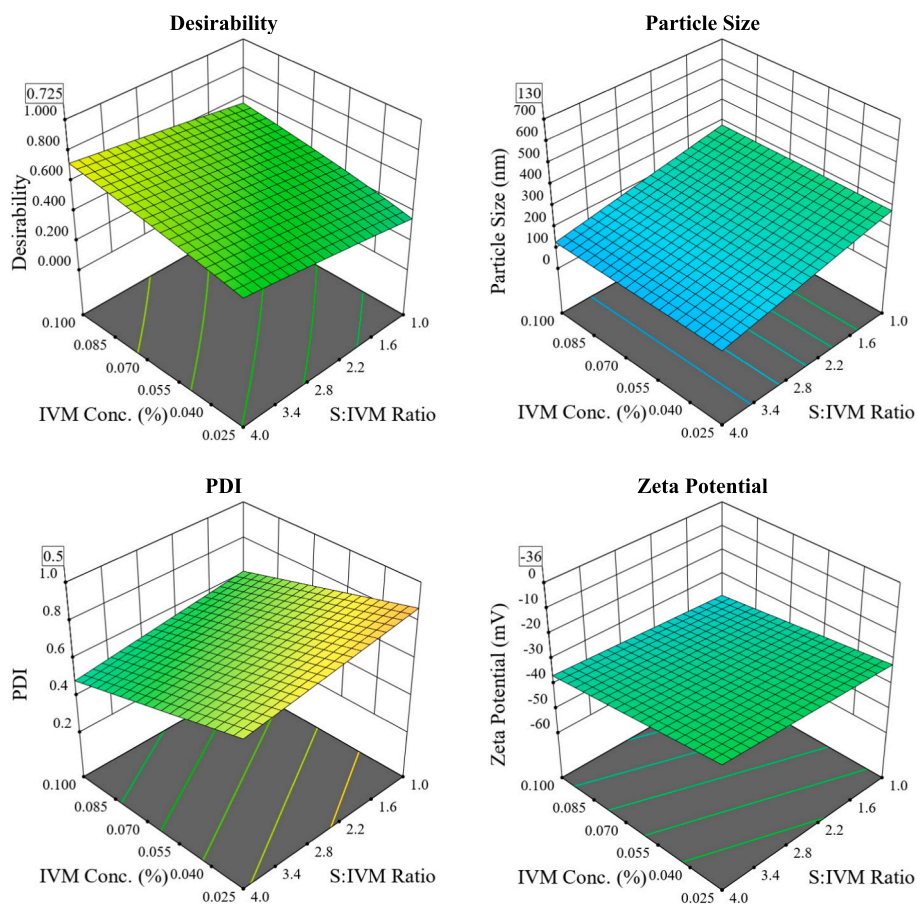


Fig. 4. Response surface plots of the desirability values and the optimum levels of the studied factors used in the optimization of IVM-NC using SDS as stabilizer.

Table 4

Predicted and observed responses of the optimized IVM-NC formulation.

Variables	Optimized Values	Responses	Predicted Values	Observed Values
X ₁	3 microfluidization cycles	Y ₁ (PS)	130.3 ± 98.16	185.9 ± 6.90
X ₂	0.1% (w/v)	Y ₂ (PDI)	0.49 ± 0.09	0.41 ± 0.04
X ₃	4:1 ratio	Y ₃ (ZP)	-36.1 ± 10.0	-44.1 ± 2.6
X ₄	SDS			
X ₅	Homogenization prior to microfluidization			

formulation exhibited a desirability value of 0.725, which indicates a high level of optimization for all the CQAs (Fig. 4).

The results suggest that utilizing a QbD approach led to the development of a straightforward method for preparing IVM-NC formulation with the desired PS (<200 nm), appropriate PDI, and ZP. After optimization, the most suitable formulation was selected for further examination. The predicted and observed responses of the optimized IVM-NC formulation are listed in Table 4. The observed values fell within the predicted values ± SD range for all responses.

After preparation, the resulting formulation was subjected to lyophilization using a matrix forming agent with cryoprotective action (1% w/v mannitol) to enhance the stability of the IVM-NC and reduce agglomeration and PS growth upon standing (Van Eerdenbrugh et al., 2008). The lyophilized powder was then subjected to comprehensive physico-chemical characterization tests. Subsequently, the powder was incorporated into a cream preparation to conduct comparable in vitro release studies with the marketed Soolantra cream.

3.3. Physico-chemical characterization of optimized IVM-NC

3.3.1. Equilibrium solubility studies

Drugs belonging to BCS Class II or Class IV, including IVM, typically have low water solubility, which often leads to a suboptimal pharmacokinetic (PK) profile for the drug. In fact, IVM is described in the USP monograph as practically insoluble in water. However, one of the most promising strategies to overcome this challenge is the development of NC. By decreasing the PS, the interfacial surface area is increased, leading to higher equilibrium solubility and dissolution rate, as predicted by the Ostwald-Freundlich and Noyes-Whitney laws.

Fig. 5 illustrates the equilibrium solubility test results for IVM-NC-L, as well as for IVM-RM, IVM-SDS-PM (in the ratio 1:4), and IVM-PVA-PM (in the ratio 1:4).

The equilibrium solubility of IVM-RM was found to be 0.00001 ± 0.000004 mg/mL, consistent with literature reports indicating an equilibrium solubility of <0.005 mg/mL (Starkloff et al., 2017; Fent, 2014). In contrast, IVM-NC-L exhibited a remarkable 730-fold increase in equilibrium solubility as compared to the IVM-RM, with a value of 0.00731 ± 0.000589 mg/mL. In the case of the physical mixtures (PM), the sample with IVM-SDS-PM in the ratio of 1:4 showed the highest

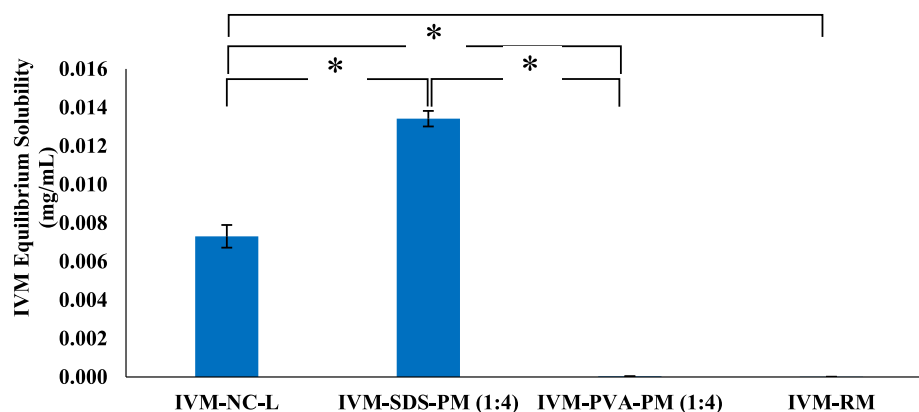


Fig. 5. Equilibrium solubility of IVM-NC-L, IVM-SDS-PM (1:4), IVM-PVA-PM (1:4), and IVM-RM in acetate buffer (pH = 5.5) at 25 °C (n = 3). * P < 0.0001.

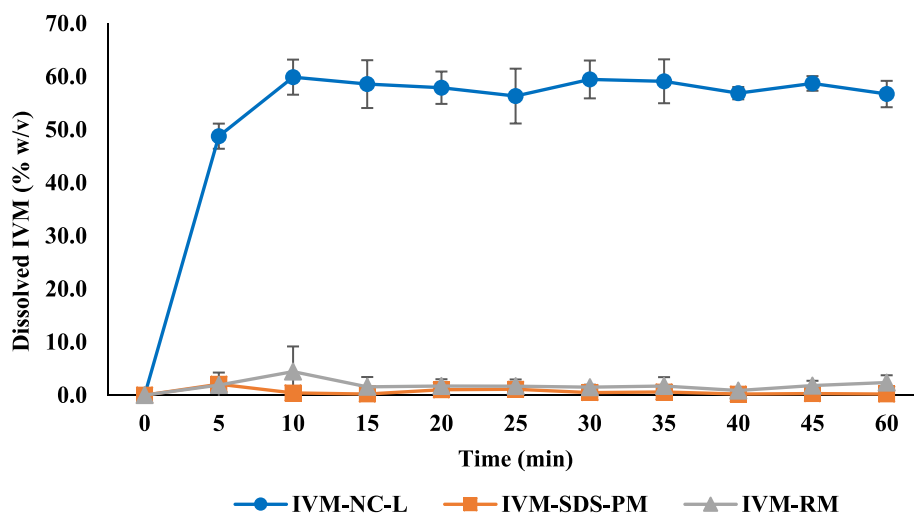


Fig. 6. In vitro dissolution profiles of IVM-NC-L, IVM-SDS-PM and IVM-RM in acetate buffer (pH = 5.5) at 32 °C (n = 3).

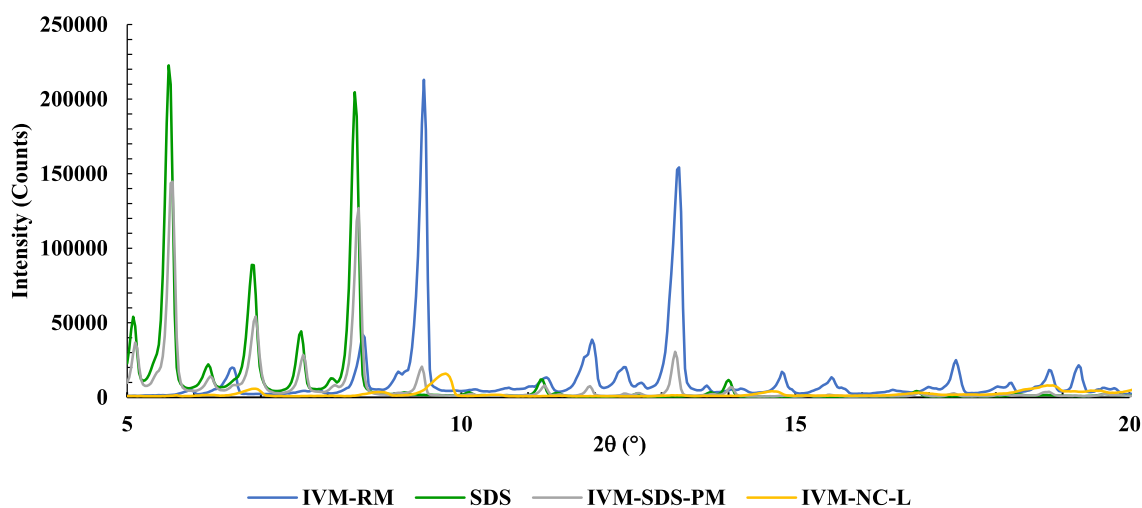


Fig. 7. XRD spectra of IVM-RM, SDS, IVM-SDS-PM (1:4) and IVM-NC-L.

solubility (0.01342 ± 0.00040 mg/mL) among all other samples. This could be attributed to the well-known ability of SDS to form micellar solution in water with a critical micelle concentration (CMC) of 7–10 mM (Hammouda, 2013). This conclusion is further supported by the results of another PM formulation, IVM-PVA-PM (1:4), which showed no significant difference from IVM-RM, as PVA lacks the ability to form

micelles. In support, a study comparing the saturation solubility of IVM-RM with PM containing different stabilizers found that physical mixtures containing SDS exhibited the highest solubility (Starkloff et al., 2017).

3.3.2. In vitro dissolution studies

Fig. 6 illustrates the in vitro dissolution profiles of the IVM-NC-L, IVM-SDS-PM and IVM-RM. The slope of the dissolution profiles allows for the determination of dissolution rates. Both the IVM-RM and IVM-SDS-PM exhibited a slow dissolution rate, while IVM-NC-L showed a significant increase in the dissolution rate and extent ($p < 0.0001$) at all intervals compared to both the IVM-RM and IVM-SDS-PM. The remarkable improvement in dissolution rate of IVM-NC, can be attributed to the enhanced solubility and increased surface-to-volume ratio in agreement with the Noyes-Whitney model (Starkloff et al., 2017). At the end of the experiment, which lasted for 60 min, the IVM-NC formulation had dissolved about 56.7% of the drug, whereas IVM-RM and IVM-SDS-PM had dissolved only 2.4% and 0.22%, respectively, indicating the superior dissolution behavior of IVM-NC-L. There was no significant difference in the dissolution profiles between the IVM-RM and IVM-SDS-PM. Although the IVM-SDS-PM showed the highest water-solubility as illustrated in section 3.3.1, it did not show improvement in the dissolution profile as compared to the IVM-RM. This can be attributed to multiple factors including the lower concentration of SDS used in the dissolution test (considering the large volume of dissolution medium) which is below the CMC. Also, below its CMC, the high affinity of SDS to water might result in salting out of dissolved IVM.

3.3.3. X-ray diffraction (PXRD)

Powder XRD studies were conducted to assess the impact of nanocrystallization on the crystallinity and structural properties of IVM. The XRD spectra of IVM-RM, SDS, IVM-SDS-PM (1:4) and IVM-NC-L are presented in Fig. 7. The pattern of IVM-RM displayed sharp distinguished peaks at multiple 2θ between 8° and 14° , at about 8.5° , 9.4° , 12° and 13.2° which confirms the crystalline nature of the raw material. The IVM-SDS-PM showed the characteristic peaks corresponding to both the IVM-RM and SDS but with reduced intensity. In contrast, the diffraction pattern of IVM-NC-L exhibited a lack of major peaks corresponding to both IVM and SDS, as well as broadening, shifting and reduction of other peaks. This suggests that the optimized IVM-NC-L formulation was amorphous, which is consistent with findings reported by Starkloff et al. regarding the dried IVM-NC suspension (Starkloff et al., 2017). The lack of SDS characteristic peaks in IVM-NC-L might indicate that a molecular dispersion between the drug and the stabilizer is formed where the overall solid becomes amorphous. The formation of an amorphous molecular dispersion provides further justification for the tremendous improvement in the observed equilibrium solubility of IVM-NC.

3.4. Morphological characterization

The TEM was employed to visualize the morphology of the optimal IVM-NC formulation in both nanosuspension and lyophilized powder forms. The TEM micrographs of the IVM-NC-S revealed that the particles were spherical with a narrow size distribution. The particles were uniformly shaped and did not display any signs of aggregation. The TEM micrograph and the DLS spectra of IVM-NC-S are shown in Fig. 8-A and B, respectively. Similarly, the TEM micrograph of the IVM-NC-L exhibited comparable characteristics, indicating that the nanosuspension remained stable during the freeze-drying process. The TEM micrograph and the DLS spectra (following redispersion) of IVM-NC-L are shown in Fig. 8-C and D, respectively.

In contrast to the IVM-NC, the IVM-RM exhibited an irregular crystalline particle shape with a size range of $6.68 \mu\text{m}$ to $15.45 \mu\text{m}$, as observed by SEM (Fig. 8-E). The significant reduction in particle size achieved through the nanocrystallization technique used in this study is crucial for improving the pharmacodynamic profile of the drug upon topical application.

3.5. Short-term physical stability study

A short-term physical stability study was conducted on both IVM-NC-

S and IVM-NC-L for three months under two different storage conditions: $25^\circ\text{C}/60\% \text{RH}$ (accelerated conditions) and $5 \pm 3^\circ\text{C}$ (long-term conditions). The results of the study are illustrated in Fig. 9. The study found that both formulations showed good stability profiles throughout the study period under both storage conditions with statistically insignificant changes related to the PS, PDI and ZP. The findings for IVM-NC-S coincide with the results of other studies that reported remarkable stability for 1% IVM-NC-S at similar accelerated conditions for six months (Starkloff et al., 2017) and indomethacin nanosuspensions stored at the same accelerated and long-term conditions for 28 days (Verma et al., 2009).

3.6. Ex vivo studies: skin permeation of IVM-NC

The water solubility of IVM is extremely poor. The goal of IVM nanocrystallization was to enhance its ability to penetrate the skin to treat parasitic infections. Nanocrystals have been found to enhance skin permeability and drug deposition compared to conventional topical formulations and applied drug solutions (Najm et al., 2022; Pelikh et al., 2018). They achieve this by augmenting the drug supersaturation solubility and increasing drug adhesion and retention time at the site of application, thus leading to a higher concentration gradient for passive diffusion of the drug (Ghasemiyeh and Mohammadi-Samani, 2020). The efficiency of IVM-NC in penetrating the skin layers was evaluated using pig ear skin. Porcine skin from the ear is commonly employed to assess transdermal drug permeation since it shares structural similarities with human skin, including hair growth density, the existence of Langerhans cells, the thickness of the SC and viable epidermis, glycosphingolipids and ceramides contents, and the arrangement of collagen fibers in the dermis (Neupane et al., 2020).

The permeation profiles of IVM-NC-S and IVM solution in acetonitrile and water (3.5:6.5) through the entire pig ear skin were compared. Fig. 10 illustrates the results, indicating that the rate and extent of IVM-NC-S permeation to the receptor chamber were lower than those of IVM solution at 2 and up to 24 h of the experiment, however, the difference was insignificant. The total percentage of IVM that permeated the skin into the receptor chamber was calculated as 34.3% for IVM-NC-S (untreated skin), 25.9% for IVM-NC-S (treated skin) and 44.8% for IVM solution.

To estimate the quantity of IVM retained in the skin, the amount of IVM remaining in the donor chamber at the end of the experiment was determined for both formulations. The results showed that IVM-NC-S using untreated or treated skin had significantly lower amount of drug left in the donor chamber, with 4.3% and 4.6 respectively, and 32.8% for IVM solution ($p < 0.05$). This might be attributed to the enhanced passive drug diffusion. Given the comparable amount of drug permeated through the skin and the significant difference in the percentage of drug left in the donor chamber, it can be estimated that the IVM retained in the skin is significantly higher for IVM-NC-S (61.3% for untreated skin and 69.5% for treated skin) compared to IVM solution (22.3%), as shown in Fig. 11. Additionally, there was no significant difference between the two IVM-NC-S sets using untreated or treated skin, which indicates that the applied organic solvent (acetonitrile in water, 3.5:6.5) was suitable and did not impact the integrity of the skin.

While a significant portion of the initial IVM solution remained in the donor chamber, possibly indicating a low concentration gradient, the majority of the dissolved drug passed through the skin into the receptor chamber and was not retained. In contrast, the IVM-NC-S showed high skin retention, indicating its potential for effectively treating skin diseases while minimizing systemic absorption. These findings suggest that a combination of optimized PS and surfactant concentration can further enhance the efficacy of NC for dermatological applications.

3.7. In vitro release of IVM-NC from topical cream

This study aimed to evaluate the release of IVM from IVM-NC cream

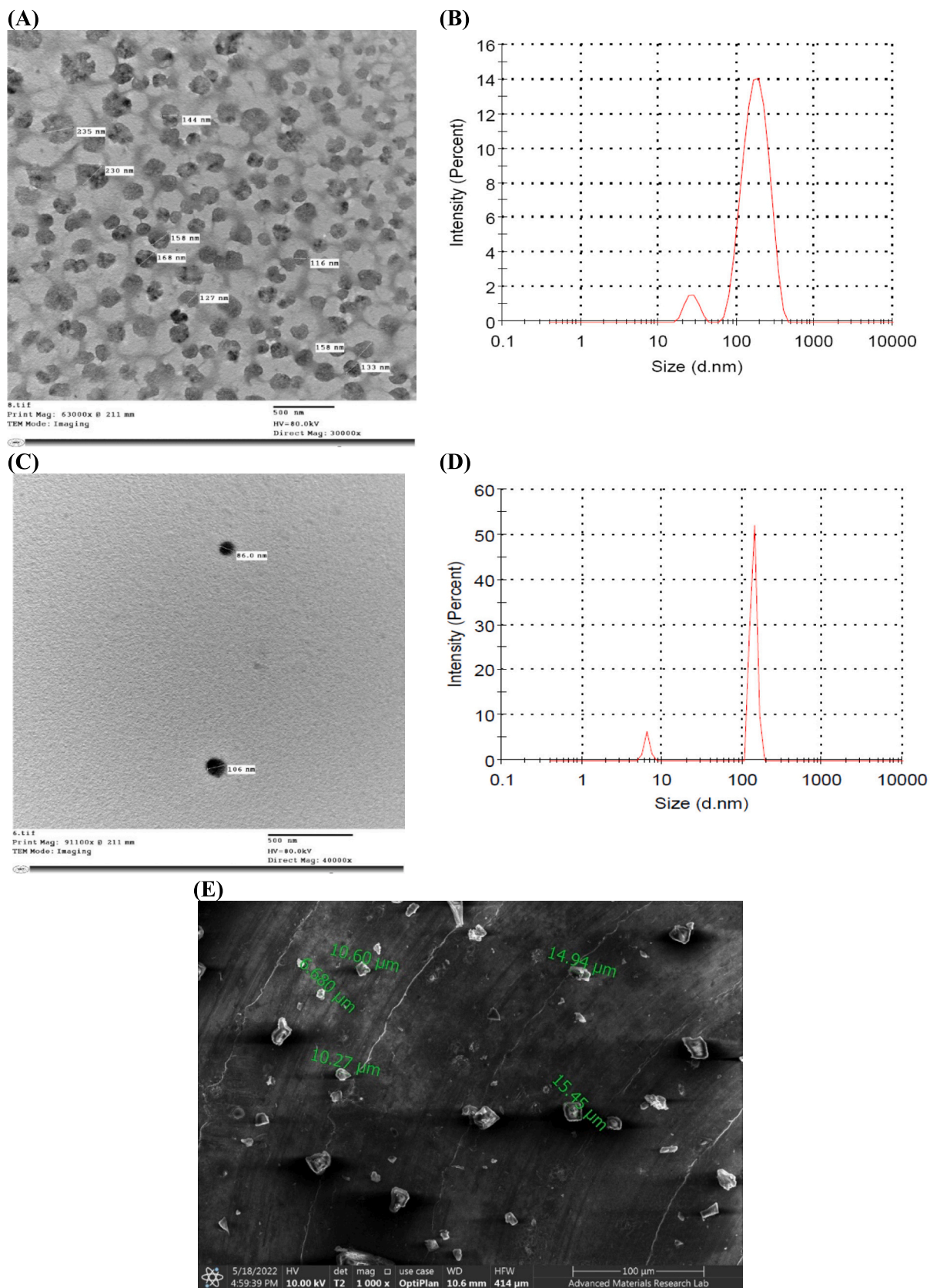


Fig. 8. TEM micrographs and DLS spectra of IVM-NC-S (A and B) and IVM-NC-L (C and D), and SEM micrograph of IVM-RM (E).

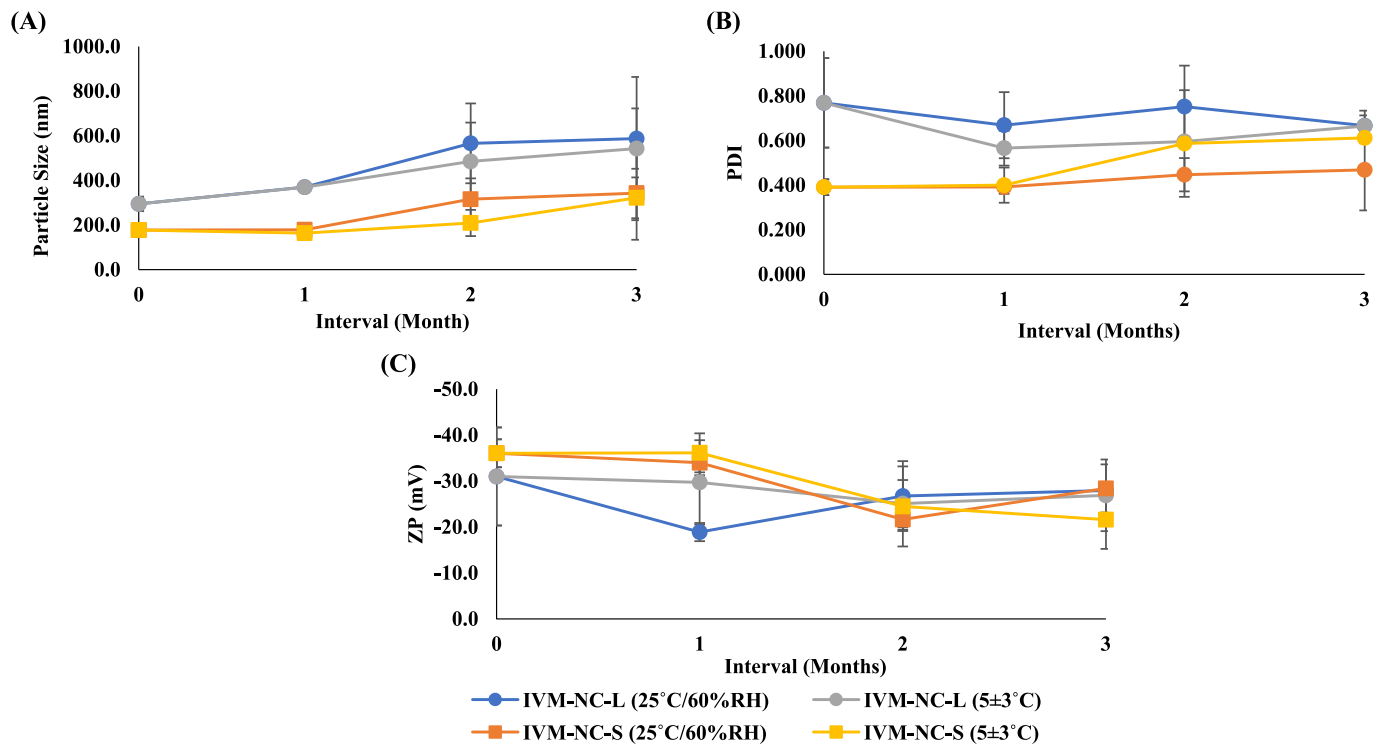


Fig. 9. Stability results for (A) PS, (B) PDI and (C) ZP for IVM-NC-S and IVM-NC-L under 25 °C/ 60 %RH and 5 ± 3 °C.

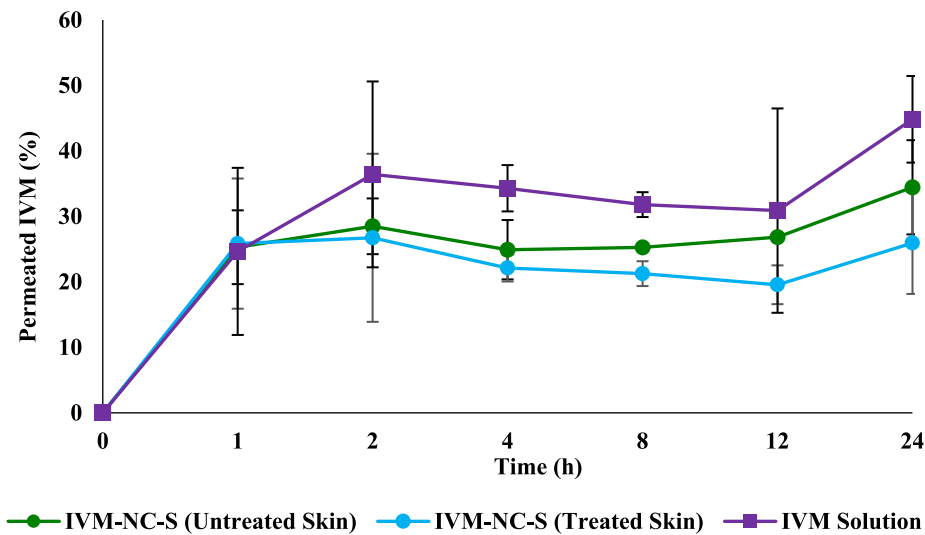


Fig. 10. Ex vivo permeation profiles of IVM-NC-S (untreated and treated skin) and IVM solution (acetonitrile in water, 3.5:6.5) through pig ear skin at 32 °C (n = 2).

in comparison to the commercially available Soolantra Cream (1% w/w IVM, Galderma, France) by incorporating IVM-NC-L into a cream preparation (1% w/w IVM). It has been reported that incorporation of NC into cream formulations enhances drug penetration into the skin particularly when compared to hydrogels or oleogels thanks to the inherent lipophilic properties of creams (Pelikh et al., 2018).

The results shown in Fig. 12 demonstrate that the IVM-NC cream exhibited a notably superior IVM release profile when compared to the Soolantra cream. Throughout a two-hour observation period, the IVM-NC cream consistently exhibited significantly higher percentages of IVM released at all time points ($p < 0.001$). For instance, after 60 min, the IVM-NC cream showed an average drug release of approximately 99%, whereas the Soolantra cream only achieved around 25% drug

release. These results support the suitability of cream as a vehicle for incorporating IVM-NC. These results are in agreement with the equilibrium solubility and dissolution results, suggesting that nanocrystallization leads to improved solubility and faster dissolution of IVM. Additionally, the use of lyophilized IVM-NC in the cream likely aided in achieving even and uniform distribution of IVM-NC in the cream, leading to quick dissolution of the drug in the cream's aqueous phase and subsequent fast release. Lyophilizates are known to enhance wettability, reduce aggregation, improve particle dispersibility, and speed up dissolution when used in a dosage form or exposed to water (Najm et al., 2022). Therefore, the incorporation of IVM-NC in a cream as a vehicle offers a potential approach to improve the efficacy of IVM in treating parasitic skin diseases.

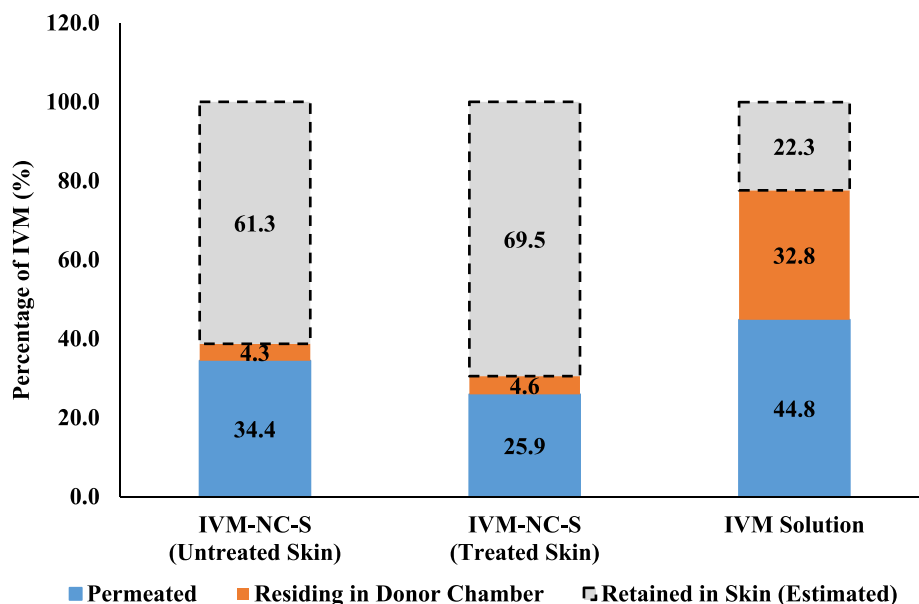


Fig. 11. The percentage of IVM permeated, residing in the donor chamber, and retained in the skin (estimated) of IVM-NC-S (untreated and treated skin) and IVM solution (acetonitrile in water, 3.5:6.5) through pig ear skin at 32 °C (n = 2).

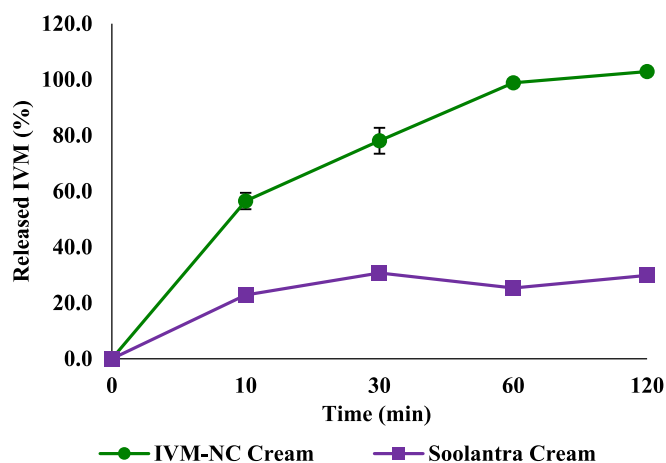


Fig. 12. In vitro release profiles of IVM from IVM-NC cream and Soolantra Cream in PBS (pH = 7.4) at 32 °C (n = 3).

In summary, NC formulations hold immense potential for effectively treating topical skin diseases due to their ability to improve skin penetration. This can be attributed to several factors including the small PS, high supersaturation solubility, rapid dissolution, and large surface to volume ratio of nanocrystals which allow for better interaction and adherence at the application site. The major route for drug penetration through the skin is the follicular pathway (Patel et al., 2018). In particular, particles with sizes ranging from 300 to 700 nm can penetrate into the hair follicle and localize deeper to form a reservoir, enhancing drug retention in the skin (Li et al., 2018). Furthermore, the presence of surfactants has been shown to act as a skin permeation enhancer by decreasing the intracellular lipid bilayers crystallinity (Parmar and Bansal, 2021). Therefore, changing the physico-chemical characteristics of IVM by nanocrystallization and lyophilization followed by its incorporation into a cream product is a promising therapeutic approach to improve the pharmacodynamic profile of IVM in topical treatment of parasitic infections.

4. Conclusion

This study highlights the great potential of IVM nanocrystals (IVM-NC) in enhancing the equilibrium solubility and dissolution rate of IVM for topical skin application. Employing the QbD approach in preparing IVM-NC using microfluidization successfully identified critical parameters, such as drug concentration, stabilizer type, and microfluidization cycles that impacted IVM-NC formation. Notably, IVM-NC showed an impressive 730-fold increase in equilibrium solubility compared to raw IVM, leading to improved dissolution rate. The optimal formulation, IVM-NC-S, demonstrated reduced drug permeation through the skin while simultaneously increasing IVM skin retention. Moreover, the release profile of IVM-NC from the prepared cream was superior to that of the commercially available Soolantra cream.

Overall, this research provides essential insights into the potential of nanocrystals in IVM formulation, offering a promising alternative to conventional topical antiparasitic products for treating skin infections. However, to fully assess the efficacy of the developed IVM-NC topical formulation compared to existing products, additional in vivo studies using an animal infection model and further microbiological investigations are essential. These studies will provide valuable data to evaluate the formulation's effectiveness and safety, helping to validate its potential as a viable treatment option for parasitic infections.

Funding

This work was supported by internal funding provided by the University of Sharjah, Sharjah, UAE (Postgraduate student project funding).

Author contributions

All authors have read and agreed to the published version of the manuscript.

CRedit authorship contribution statement

Hoda Awad: Methodology, Software, Data curation, Formal analysis, Investigation, Writing – original draft. **Mutasem Rawas-Qalaji:** Formal analysis, Validation, Writing – review & editing. **Rania El**

Hosary: Investigation, Formal analysis, Writing – review & editing.
Jayalakshmi Jagal: Methodology, Formal analysis. **Iman Saad Ahmed:** Project administration, Supervision, Conceptualization, Formal analysis, Validation, Writing – review & editing, Funding acquisition.

Declaration of Competing Interest

The authors declare no conflict of interest.

Data availability

Data will be made available on request.

Acknowledgement

The authors thank our fellow colleague at University of Sharjah, Mona Najm, for her assistance and contribution. We also thank Hovione PharmaScience Limited (Taipa, Macau) for gifting us the Ivermectin raw material.

References

- Agrawal, U., Mehra, N.K., Gupta, U., Jain, N.K., 2013. Hyperbranched dendritic nano-carriers for topical delivery of dithranol. *J. Drug Target.* 21 (5), 497–506. <https://doi.org/10.3109/1061186X.2013.771778>, 2013/05/01.
- Ahmed, I.S., El Hosary, R., Hassan, M.A., Haider, M., Abd-Rabo, M.M., 2018. Efficacy and safety profiles of oral atorvastatin-loaded nanoparticles: effect of size modulation on biodistribution. *Mol. Pharm.* 15 (1), 247–255. <https://doi.org/10.1021/acs.molpharmaceut.7b00856>, 2018/01/02.
- Ahmed, I.S., Elnahas, O.S., Assar, N.H., Gad, A.M., El Hosary, R., Feb 25 2020. Nanocrystals of fusidic acid for dual enhancement of dermal delivery and antibacterial activity: in vitro, ex vivo and in vivo evaluation. *Pharmaceutics* 12 (3). <https://doi.org/10.3390/pharmaceutics12030199>.
- Al Jalali, V., Zeitlinger, M., Jul 2020. Systemic and Target-site pharmacokinetics of antiparasitic agents. *Clin. Pharmacokinet.* 59 (7), 827–847. <https://doi.org/10.1007/s40262-020-00871-5>.
- Aodah, A., Bafail, R.S., Rawas-Qalaji, M., Jul 2017. Formulation and evaluation of fast-disintegrating sublingual tablets of atropine sulfate: the effect of tablet dimensions and drug load on tablet characteristics. *AAPS PharmSciTech* 18 (5), 1624–1633. <https://doi.org/10.1208/s12249-016-0631-y>.
- Atmakuri, S., Nene, S., Khatri, D., Singh, S.B., Sinha, V.R., Srivastava, S., 2023. Forging ahead the repositioning of multitargeted drug ivermectin. *Curr. Drug Deliv.* 20 (8), 1049–1066. <https://doi.org/10.2174/1567201819666220516163242>.
- Bafail, R., Rawas-Qalaji, M., Rawas-Qalaji, M., Aodah, A., Oct 2019. Effect of the filler grade on the characteristics and the sublingual permeability of atropine sulfate fast disintegrating sublingual tablets. *Drug Dev. Ind. Pharm.* 45 (10), 1617–1623. <https://doi.org/10.1080/03639045.2019.1648499>.
- Bruschi, F., Sep 2014. The challenge of antiparasitic resistance. *J. Glob. Antimicrob. Resist.* 2 (3), 131–132. <https://doi.org/10.1016/j.jgar.2014.06.002>.
- CDC - Neglected Tropical Diseases, 2023. Centers for Disease Control and Prevention. Updated 7 March. Accessed 26 April 2023. <https://www.cdc.gov/globalhealth/ntd/diseases/index.html>.
- Clogston, J.D., Patri, A.K., 2011. Zeta potential measurement. *Methods Mol. Biol.* 697, 63–70. https://doi.org/10.1007/978-1-60327-198-1_6.
- Da, D., 2015. Study on Ivermectin Nanoemulsion for Transdermal Drug Delivery. *China Animal Husbandry & Veterinary Medicine*.
- Das, S., Lee, S.H., Chia, V.D., et al., May 2020. Development of microemulsion based topical ivermectin formulations: Pre-formulation and formulation studies. *Colloids Surf. B: Biointerfaces* 189, 110823. <https://doi.org/10.1016/j.colsurfb.2020.110823>.
- Dragicevic, N., Maibach, H. (Eds.), 2016. *Percutaneous Penetration Enhancers Chemical Methods in Penetration Enhancement*, 1 ed. Springer.
- D'Souza, S., 2014. A review of in vitro drug release test methods for nano-sized dosage forms. *Adv. Pharm.* <https://doi.org/10.1155/2014/304757>, 2014/11/20 2014. 304757.
- Fent, G.M., 2014. Ivermectin. In: *Wexler, P. (Ed.), Encyclopedia of Toxicology (Third Edition)*. Academic Press, pp. 342–344.
- Ghasemiyeh, P., Mohammadi-Samani, S., 2020. Potential of nanoparticles as permeation enhancers and targeted delivery options for skin: advantages and disadvantages. *Drug Des. Devel. Ther.* 14, 3271–3289. <https://doi.org/10.2147/dddt.S264648>.
- Gigliobianco, M.R., Casadidio, C., Censi, R., Di Martino, P., Aug 21 2018. Nanocrystals of poorly soluble drugs: drug bioavailability and physicochemical stability. *Pharmaceutics*. 10 (3) <https://doi.org/10.3390/pharmaceutics10030134>.
- Guo, D., Dou, D., Li, X., Zhang, Q., Bhatto, Z.A., Wang, L., 2018. Ivermectin-loaded solid lipid nanoparticles: preparation, characterisation, stability and transdermal behaviour. *Artificial Cells, Nanomed. Biotechnol.* 46 (2), 255–262. <https://doi.org/10.1080/21691401.2017.1307207>, 2018/02/17.
- Hammouda, B., 2013. Temperature effect on the Nanostructure of SDS Micelles in Water. *J. Res. Natl. Inst. Stand. Technol.* 118, 151–167. <https://doi.org/10.6028/jres.118.008>.
- Heukelbach, J., Walton, S.F., Feldmeier, H., 2005. Ectoparasitic infestations. *Curr. Infect. Dis. Rep.* 7 (5), 373–380. <https://doi.org/10.1007/s11908-005-0012-2>, 2005/09/01.
- Huh, A.J., Kwon, Y.J., 2011. “Nanoantibiotics”: a new paradigm for treating infectious diseases using nanomaterials in the antibiotics resistant era. *J. Control. Release* 156 (2), 128–145. <https://doi.org/10.1016/j.jconrel.2011.07.002>, 2011/12/10/.
- Junghanns, J.U., Müller, R.H., 2008. Nanocrystal technology, drug delivery and clinical applications. *Int. J. Nanomedicine* 3 (3), 295–309. <https://doi.org/10.2147/ijn.s595>.
- Kalhapure, R.S., Suleman, N., Mocktar, C., Seedat, N., Govender, T., Mar 2015. Nanoengineered drug delivery systems for enhancing antibiotic therapy. *J. Pharm. Sci.* 104 (3), 872–905. <https://doi.org/10.1002/jps.24298>.
- Küchler, S., Radowski, M.R., Blaschke, T., et al., 2009. Nanoparticles for skin penetration enhancement – a comparison of a dendritic core-multishell-nanotransporter and solid lipid nanoparticles. *Eur. J. Pharm. Biopharm.* 71 (2), 243–250. <https://doi.org/10.1016/j.ejpb.2008.08.019>, 2009/02/01/.
- Lademann, J., Richter, H., Teichmann, A., et al., May 2007. Nanoparticles—an efficient carrier for drug delivery into the hair follicles. *Eur. J. Pharm. Biopharm.* 66 (2), 159–164. <https://doi.org/10.1016/j.ejpb.2006.10.019>.
- Li, Y., Wang, D., Lu, S., et al., Nov 1 2018. Pramipexole nanocrystals for transdermal permeation: characterization and its enhancement micro-mechanism. *Eur. J. Pharm. Sci.* 124, 80–88. <https://doi.org/10.1016/j.ejps.2018.08.003>.
- Lipsky, B.A., Hoey, C., Nov 15 2009. Topical antimicrobial therapy for treating chronic wounds. *Clin. Infect. Dis.* 49 (10), 1541–1549. <https://doi.org/10.1086/644732>.
- Liu, Y., Zhao, J., Chen, J., Miao, X., Jul 2023. Nanocrystals in cosmetics and cosmeceuticals by topical delivery. *Colloids Surf. B: Biointerfaces* 227, 113385. <https://doi.org/10.1016/j.colsurfb.2023.113385>.
- Mishra, P.R., Al Shaal, L., Müller, R.H., Keck, C.M., Apr 17 2009. Production and characterization of Hesperetin nanosuspensions for dermal delivery. *Int. J. Pharm.* 371 (1–2), 182–189. <https://doi.org/10.1016/j.ijpharm.2008.12.030>.
- Müller, R.H., Gohla, S., Keck, C.M., May 2011. State of the art of nanocrystals—special features, production, nanotoxicology aspects and intracellular delivery. *Eur. J. Pharm. Biopharm.* 78 (1), 1–9. <https://doi.org/10.1016/j.ejpb.2011.01.007>.
- Najm, M.B., Rawas-Qalaji, M., Assar, N.H., Yahia, R., Hosary, R.E., Ahmed, I.S., Sep 1 2022. Optimization, characterization and in vivo evaluation of micro-pirocin nanocrystals for topical administration. *Eur. J. Pharm. Sci.* 176, 106251 <https://doi.org/10.1016/j.ejps.2022.106251>.
- Neupane, R., Bodd, S.H.S., Renukuntla, J., Babu, R.J., Tiwari, A.K., Feb 13 2020. Alternatives to biological skin in permeation studies: current trends and possibilities. *Pharmaceutics* 12 (2). <https://doi.org/10.3390/pharmaceutics12020152>.
- Nidhi, R., Rahul, M., Dnyaneshwar, K., Susanne, R.Y.-O., Mahavir, B.C., Rakesh, K.T., 2019. Chapter 10 - Importance of physicochemical characterization of nanoparticles in pharmaceutical product development. In: Rakesh, K.T. (Ed.), *Basic Fundamentals of Drug Delivery*. Academic Press, pp. 369–400 vol. *Advances in Pharmaceutical Product Development and Research*.
- Oscar, E.-R., Paulina, F.-V., Samantha, J.-X., Carlos, G.G.-T., Susana, M.-E., David, Q.-G., 2019. Rapamycin-loaded polyborate 80-coated PLGA nanoparticles: Optimization of formulation variables and in vitro anti-glioma assessment. *J. Drug Deliv. Sci. Technol.* 52, 488–499. <https://doi.org/10.1016/j.jddst.2019.05.026>.
- Parmar, P.K., Bansal, A.K., 2021. Novel nanocrystal-based formulations of apremilast for improved topical delivery. *Drug Deliv. Translat. Res.* 11 (3), 966–983. <https://doi.org/10.1007/s13346-020-00809-1>, 2021/06/01.
- Patel, V., Sharma, O.P., Mehta, T., Apr 2018. Nanocrystal: a novel approach to overcome skin barriers for improved topical drug delivery. *Expert Opin. Drug Deliv.* 15 (4), 351–368. <https://doi.org/10.1080/17425247.2018.1444025>.
- Patzelt, A., Richter, H., Knorr, F., et al., Feb 28 2011. Selective follicular targeting by modification of the particle sizes. *J. Control. Release* 150 (1), 45–48. <https://doi.org/10.1016/j.jconrel.2010.11.015>.
- Pelikh, O., Stahr, P.L., Huang, J., et al., Jul 2018. Nanocrystals for improved dermal drug delivery. *Eur. J. Pharm. Biopharm.* 128, 170–178. <https://doi.org/10.1016/j.ejpb.2018.04.020>.
- Purohit, D., Sharma, S., Lamba, A.K., et al., 2023. Nanocrystals: a deep insight into formulation aspects, stabilization strategies, and biomedical applications. *Recent Pat. Nanotechnol.* 17 (4), 307–326. <https://doi.org/10.2174/1872210516666220523120313>.
- Rawas-Qalaji, M.M., Werdy, S., Rachid, O., Simons, F.E., Simons, K.J., Oct 2015. Sublingual diffusion of epinephrine microcrystals from rapidly disintegrating tablets for the potential first-aid treatment of anaphylaxis: in vitro and ex vivo study. *AAPS PharmSciTech* 16 (5), 1203–1212. <https://doi.org/10.1208/s12249-015-0306-0>.
- Sharma, G., Goyal, H., Thakur, K., Raza, K., Katar, O.P., Oct 2016. Novel elastic membrane vesicles (EMVs) and ethosomes-mediated effective topical delivery of aceclofenac: a new therapeutic approach for pain and inflammation. *Drug Deliv.* 23 (8), 3135–3145. <https://doi.org/10.3109/10717544.2016.1155244>.
- Sharun, K., Shyamkumar, T.S., Aneesa, V.A., Dhama, K., Pawde, A.M., Pal, A., Aug 2019. Current therapeutic applications and pharmacokinetic modulations of ivermectin. *Vet World.* 12 (8), 1204–1211. <https://doi.org/10.14202/vetworld.2019.1204-1211>.

- Shen, G., Liu, M., Wang, Z., Wang, Q., Sep 29 2018. Hierarchical Structure and Catalytic activity of Flower-like CeO₂ Spheres prepared Via a Hydrothermal Method. *Nanomaterials (Basel)*. 8 (10) <https://doi.org/10.3390/nano8100773>.
- Sheshala, R., Anuar, N.K., Abu Samah, N.H., Wong, T.W., Apr 15 2019. In vitro drug dissolution/permeation testing of nanocarriers for skin application: a comprehensive review. *AAPS PharmSciTech* 20 (5), 164. <https://doi.org/10.1208/s12249-019-1362-7>.
- Starkloff, W.J., Bucalá, V., Palma, S.D., Gonzalez Vidal, N.L., 2017. Design and in vitro characterization of ivermectin nanocrystals liquid formulation based on a top-down approach. *Pharm. Dev. Technol.* 22 (6), 809–817. <https://doi.org/10.1080/10837450.2016.1200078>, 2017/08/18.
- Sun, Y., Chen, D., Pan, Y., et al., Dec 2019. Nanoparticles for antiparasitic drug delivery. *Drug Deliv.* 26 (1), 1206–1221. <https://doi.org/10.1080/10717544.2019.1692968>.
- Tizek, L., Schielein, M.C., Seifert, F., Biedermann, T., Bohner, A., Zink, A., Jul 2019. Skin diseases are more common than we think: screening results of an unreferral population at the Munich Oktoberfest. *J. Eur. Acad. Dermatol. Venereol.* 33 (7), 1421–1428. <https://doi.org/10.1111/jdv.15494>.
- Ullio-Gamboa, G., Palma, S., Benoit, J.P., Allemandi, D., Picollo, M.I., Toloza, A.C., Aug 2017. Ivermectin lipid-based nanocarriers as novel formulations against head lice. *Parasitol. Res.* 116 (8), 2111–2117. <https://doi.org/10.1007/s00436-017-5510-2>.
- USP, 2020. Ivermectin Official Monograph. *The United States Pharmacopeia and National Formulary (USP 43-NF 38)*. 12601 Twinbrook Parkway. United States Pharmacopeial Convention, Rockville, MD 20852, USA, pp. 2470–2472.
- Van Eerdenbrugh, B., Van den Mooter, G., Augustijns, P., 2008. Top-down production of drug nanocrystals: Nanosuspension stabilization, miniaturization and transformation into solid products. *Int. J. Pharm.* 364 (1), 64–75. <https://doi.org/10.1016/j.ijpharm.2008.07.023>, 2008/11/19/.
- Verma, S., Lan, Y., Gokhale, R., Burgess, D.J., 2009. Quality by design approach to understand the process of nanosuspension preparation. *Int. J. Pharm.* 377 (1), 185–198. <https://doi.org/10.1016/j.ijpharm.2009.05.006>, 2009/07/30/.
- Xing, M., Zhong, W., Xu, X., Thomson, D., Jul 20 2010. Adhesion force studies of nanofibers and nanoparticles. *Langmuir*. 26 (14), 11809–11814. <https://doi.org/10.1021/la100443d>.